Domain wall engineering through exchange bias

E. Albisetti[1] and D. Petti[1]

[1]Dipartimento di Fisica, Politecnico di Milano, Via Giuseppe Colombo 81, 20133 Milano, Italy

Corresponding Author:

Edoardo Albisetti,

edoardo.albisetti@polimi.it

PoliFab - Department of Physics - Politecnico di Milano

Via Giuseppe Colombo 81, 20133 Milano, Italy

Office +39 0223999659

Abstract

The control of the structure and position of magnetic domain walls is at the basis of the development of different magnetic devices and architectures. Several nanofabrication techniques have been proposed to geometrically confine and shape domain wall structures; however, a fine tuning of the position and micromagnetic configuration is hardly achieved, especially in continuous films. This work shows that, by controlling the unidirectional anisotropy of a continuous ferromagnetic film through exchange bias, domain walls whose spin arrangement is generally not favored by dipolar and exchange interactions can be created. Micromagnetic simulations reveal that the domain wall width, position and profile can be tuned by establishing an abrupt change in the direction and magnitude of the exchange bias field set in the system.

Keywords

Magnetic Domain Wall, Néel Domain Wall, Exchange Bias, Micromagnetic simulation, Magnetic Domain

1. Introduction

Magnetic domain walls (DWs) have attracted great interest in recent years, both in fundamental studies [1][2] and for their application as building blocks in different devices, such as magnetic logic circuits [3], magnetic memories [4] or magnetic microfluidic platforms [5]. In such applications, the ability to control the DW configuration is fundamental. Several studies proposed to use nanofabrication techniques in order to geometrically control the domain wall width and shape [6]. Artificially induced defects are used as pinning sites [7],[8], while nanopatterned structures provide modification of the DWs configuration, size and dynamic properties [9], [10], [11],[12].

These latter approaches are based on the competition between exchange energy and magnetostatic energy, which influence the structure of the wall. However, in a continuous film or bulk material, the DW structure is predominantly ruled by materials parameters, making the DW engineering rather difficult. One solution is based on the oblique evaporation of ferromagnetic thin strips, which provide a control on the uniaxial magnetic anisotropy of the film and thus allows to manipulate the orientation of magnetic domains and domain walls [13]. Moreover, the film morphology influences the demagnetizing factor and thus the domain wall thickness and coercivity [14]. However, these methods in most cases do not allow a fine control on the domain wall position and spin configuration.

In the following, a different approach is proposed where, by spatially controlling the exchange bias [15] both in magnitude and direction, regions characterized by different unidirectional anisotropy are created within a continuous film. This allows a fine control on the position of the domain wall, which in the studied system generally nucleates at the regions boundary, and on the spatial profile of the spin orientation across the wall.

Exchange bias has been proposed to create DW pinning sites enabling the development of solid state magnetic memories [16]. Using crossed ferromagnetic and antiferromagnetic wires such that exchange bias can be introduced at the intersection, pinning field strength up to 37 Oe has been achieved.

Conversely, this paper proposes to exploit exchange bias in order to promote the nucleation of Néel domain walls in a thin continuous film. Micromagnetic simulations show that in a prototypal exchanged bias system, domain wall width in the 1 μm-150 nm range can be obtained at the boundary between two regions with opposite exchange bias field ranging from 50 to 300 Oe. These exchange bias values are compatible with those found in the $Fe_{40}Co_{40}B_{20}/Ir_{20}Mn_{80}$ or $Py/Ir_{20}Mn_{80}$ systems [17], [18],[19].

Moreover, by tuning the direction and strength of the exchange bias within the regions, different spin orientations, asymmetric spin profiles and controlled shifts of the domain wall can be achieved. The possibility to easily control domain wall properties such as width, spin structure and position paths the way to the design of novel domain wall-based magnetic devices.

2. Computational details

Micromagnetic simulations were performed using Object Oriented MicroMagnetic Framework (OOMMF) platform [20]. A 5 nm CoFeB layer was simulated, modeling the exchange bias as an external field. Any variation of exchange bias field caused by the reorientation of the antiferromagnetic moments due to the antiferromagnetic/ferromagnetic exchange coupling is neglected. Such an approximation is justified in polycrystalline exchange bias systems characterized by large antiferromagnetic uniaxial anisotropy (e.g. ($Fe_{40}Co_{40}B_{20}$/$Ir_{20}Mn_{80}$ systems grown by magnetron sputtering) [21]. The studied structure is depicted in Fig. 1: the simulated area was divided into two regions characterized by the same magneto-crystalline anisotropy, but by different directions and intensities of the exchange bias field, named H_{eb1} and H_{eb2} in both panels. An abrupt change of exchange bias field H_{eb} at the interface between the two regions was considered. This assumption is reasonable e.g. in polycrystalline exchanged bias systems, where the antiferromagnetic film presents non-interacting single domain grains [21].

The parameters employed for the simulations were: cell size 10 nm x 10 nm x 5 nm, saturation magnetization M_s = 750 kA/m, damping coefficient α = 0.5 and exchange stiffness A_{ex} = 1.2 10^{-11} J/m [22], [23]. The uniaxial anisotropy was neglected, apart from the simulations of Fig. 4, where a uniaxial anisotropy constant K = 10^3 J/m^3 was considered with easy-axis lying in the x or y direction. A 5x5 μm^2 square-shaped area was considered in the simulation. In order to minimize the effect of the boundaries, the magnetization at the vertical (y direction) edges of the simulated area was fixed in the direction of the applied exchange bias.

In all simulations, the magnetization was initially set in saturation along the +y direction and +x direction for configuration A and B, respectively. The system was then let to relax in 0 applied magnetic field.

Starting from the equilibrium micromagnetic configuration, the spin angle $\theta(x)$ was calculated as:

$$\theta(x) = \arctan\left(\frac{M_{\mathrm{par}}(x)}{M_{\mathrm{perp}}(x)}\right) \qquad (1)$$

Where $M_{\mathrm{par}}(x)$ and $M_{\mathrm{perp}}(x)$ represent the magnetization components oriented in the parallel and perpendicular direction with respect to the exchange bias direction (red arrows in Fig.1), respectively, as a function of the distance x from the center of the simulated area (see e.g. Fig.2a).

The domain wall width was determined starting from the spin angle function and considering the following definition [24], which is valid even in case of asymmetric and non-uniform variations of $\theta(x)$:

$$\delta_{DW} = \int_{-\infty}^{+\infty} \theta(x)dx \qquad (2)$$

3. Results and discussion

The equilibrium micromagnetic configuration in remanence, i.e., when no external magnetic field is applied, was simulated for different values and orientations of the exchange bias fields H_{eb1} and H_{eb2} in the two regions of the sample. The red arrows in Fig. 1 show two different configurations for the exchange bias: in (a), the exchange bias H_{eb1} lies along the +*x* direction, while H_{eb2} along –*x* (conf. A); in (b), the exchange bias H_{eb1} lies along the +*y* direction, while H_{eb2} along –*y* (conf. B). The magnetization within each region (grey arrows in Fig. 1) results uniformly oriented along the exchange bias direction, giving rise to two well-defined ferromagnetic domains. In the proximity of the regions boundaries, the magnetization rotates from one configuration to the other, giving rise to a domain wall whose properties are determined by the interplay between exchange interaction, dipolar interaction, uniaxial anisotropy and exchange bias.

In Fig. 2, the micromagnetic structure of the DW in conf. A is studied, as a function of the exchange bias field strength, with $H_{eb1} = -H_{eb2}$ ranging from 50 Oe to 300 Oe. For better studying the influence of the exchange bias field on the DW structure, a 0 uniaxial anisotropy was considered in this simulation. Such condition can be experimentally obtained by employing ferromagnetic materials with a low magnetocrystalline anisotropy such as Permalloy (Py). In Fig. 2a the micromagnetic configuration of the structure is plotted as a function of the distance from the regions boundary ranging from -800 nm to +800 nm, for different exchange bias fields. It can be observed that the magnetization (black arrows) lies along the +*x* direction for x<<0, rotates coherently in proximity of the region boundary (*x*=0) within the plane of the film, and finally lies along the –*x* direction for x>>0, determining the so-called head-to-head Néel DW. The orange color saturation is proportional to M_y, so that the domain wall region is easily identified. The domain wall is located exactly at the interface between the two exchange biased regions (dashed line in Fig. 1a), due to the fact that the exchange bias field is symmetric, i.e., has the same absolute value in the two regions. It is clear that the spatial extension of the domain wall, in this configuration, is strongly dependent on the exchange bias field. In particular, the DW width is lower for larger values of exchange bias, due to the fact that a large exchange bias field induces a stronger alignment of the magnetization along the –*x*/+*x* directions, shrinking the region where the magnetization is let to rotate.

In Fig. 2b, the normalized *x* and *y* components of the magnetization M_x and M_y, empty and filled symbols, respectively, are plotted as a function of *x*. It can be observed that M_y is maximum and equal to 1 in correspondence of *x*=0, i.e., on the boundary of the exchange biased regions. Furthermore, in the same position, M_x=0. This indicates that, for *x*=0, the magnetization is fully oriented along the DW. The spin orientation within the DW is further clarified in Fig.2c, where the spin angle is plotted as a function of *x* for different exchange bias fields. As already discussed in the previous section, the spin angle $\theta(x)$ is defined starting from $M_{par}(x)$ and $M_{perp}(x)$, where, in this configuration $M_{par}(x) = M_x(x)$ and $M_{perp}(x) = M_y(x)$, resulting in $\theta(x) = \operatorname{artan}\left(\frac{M_x(x)}{M_y(x)}\right)$. It can be observed that the spin angle varies continuously from -90° to +90° and is

0° at *x*=0. The steepness of the curve is directly related to the strength of the exchange bias field, so that larger exchange bias leads to a steeper transition.

It is worth noting that, from the energetic point of view, the presence of a head-to-head DW in a continuous film is usually unfavorable due to the strong demagnetizing field which arises in this configuration. Therefore, the particular geometry of the exchange bias in this case is crucial for nucleating the domain wall and determining its position, width and spin configuration.

Fig. 3 shows the micromagnetic configuration of the domain wall in conf. B, i.e., when the exchange bias is oriented along +*y* and –*y.* No uniaxial anisotropy was considered. Contrarily to the former case, H_{eb} lies parallel to the region boundary, and so does the magnetization within the two domains. In the regions boundary, the magnetization rotates coherently in the film plane, giving rise to a Néel wall. Fig.3a shows the micromagnetic configuration for exchange bias field ranging from 50 Oe to 300 Oe, and *x* from -420 nm to 420 nm. The color saturation is proportional to M_x. For *x*=0, the magnetization lies along +*x*, i.e., is perpendicular to the DW, whereas, away from the boundary, the magnetization lies along the exchange bias direction. Fig.3b-c show M_x, M_y and θ as a function of *x*. The spin angle in this configuration is defined as $\theta(x) = \arctan\left(\frac{M_y(x)}{M_x(x)}\right)$. It is clear that for larger exchange bias field, the spatial profile of the spin rotation is steeper, leading to a narrower DW. However, it is worth noting that, with respect to the configuration shown in Fig.2, the DW in this case is much narrower, and less influenced by the exchange bias field strength. In particular, as shown both in Fig 3a and Fig 3c, the spatial profile of the magnetization and the spin angle are only slightly affected by the exchange bias field. This is due to the fact that, in this configuration, the DW is already stabilized by the demagnetizing field, so that the exchange bias acts as a slight modulation of the ground state.

In Fig. 4a-b the combined effect of the exchange bias and uniaxial anisotropy is studied in conf. A and B, respectively. The DW width, calculated as stated in the introduction, is plotted as a function of the exchange bias field and *K*. The effect of the uniaxial anisotropy on the domain wall properties was studied by running the same set of simulations as the ones shown in Fig. 2 and Fig.3, considering a uniaxial anisotropy constant $K=10^3$ J/m^3, and both *x* and *y* as easy uniaxial anisotropy directions. This uniaxial anisotropy constant is consistent for instance with the magnetocrystalline anisotropy values of thin $Fe_{40}Co_{40}B_{20}$ films [23].

Fig. 4a presents the results in the case of conf. A. The black line shows the case of no uniaxial anisotropy (*K*=0). The DW width is reduced from 680 nm to 160 nm. When the uniaxial anisotropy is set perpendicularly to the exchange bias direction (red line), the DW width is larger (ranging from 1100 nm to 180 nm), due to the fact that the uniaxial anisotropy interaction tends to favor the alignment of the magnetization along *y*, inducing a more gradual spatial variation of the magnetization. On the contrary, when the uniaxial anisotropy is set along *x* (blue line), i.e., parallel to the exchange bias direction, it promotes a narrower domain wall,

ranging from 500 nm to 180 nm. It is worth noting that the difference in the DW width due to the uniaxial anisotropy is significant only for low exchange bias fields. This is consistent with the fact that for larger exchange bias, the shape and properties of the DW are only slightly modified by the additional anisotropy term.

Fig. 4b shows the results in the case of conf. B. In absence of uniaxial anisotropy (K=0), the domain wall width ranges from 470 nm to 145 nm. In analogy with the former case, for all the exchange bias values, the DW is narrower (from 360 nm to 145 nm) when the uniaxial anisotropy is set along the exchange bias direction (along y), and wider (from 690 nm to 160 nm) when the uniaxial anisotropy is set perpendicular to the exchange bias direction (along x). Furthermore, consistently with what observed in Fig.2 and Fig.3, the effect of the anisotropy on the DW width is reduced with respect to the first configuration, due to the stabilizing effect of the demagnetizing field.

Fig. 5 and Fig. 6 show the effect of the asymmetry of the exchange bias on the shape and width of the DW, in conf. A and B, respectively. In particular, for each configuration, the exchange bias field H_{eb1} was swept from 50 Oe to 300 Oe, while H_{eb2} was swept from -300 Oe to -50 Oe. No uniaxial anisotropy was considered in these simulations. This peculiar asymmetric configuration can be obtained experimentally by ion irradiation techniques, by modulating the ions dose for selectively destroying or weaken the exchange coupling between the antiferromagnetic and ferromagnetic layers and therefore the exchange bias [25].

Fig. 5a shows the spin structure of the DW in conf. A for different exchange bias field, as a function of x. It is clear that the asymmetry in the exchange bias reflects in a change in the DW shape and width. In particular, in the region with lower exchange bias, the spin rotation occurs over a larger distance. This leads to a shift of the DW towards the region with lower exchange bias, and to an asymmetry in the spin angle profile as shown in Fig. 5b. The inset of Fig.5b shows the DW width and shift x_0, as a function of H_{eb1}. x_0, defined as the distance of the DW center from the regions boundary, ranges from -100 nm to +100 nm, when H_{eb1} is swept from 50 Oe to 300 Oe and H_{eb2} from -300 Oe to -50 Oe. The DW width ranges from about +500 nm to -500 nm.

Fig. 6 shows the micromagnetic structure (a) and spin angle profile (b) for the conf. B. The exchange bias field range is the same as in Fig. 5. In the inset, the DW position x_0 and width as a function of H_{eb1} are shown. Consistently with what observed before, the DW shape and width are less affected by the exchange bias asymmetry with respect to the former case. In particular, x_0 ranges from around -30 nm to 30 nm across the entire exchange bias field range, while the domain wall width ranges from about + 300 nm to -300 nm.

4. Conclusions

In this paper, micromagnetic simulations show that a fine tuning of the DW position, micromagnetic configuration and properties, such as width and spin rotation, can be achieved by spatially modulating the exchange bias across the sample, in a continuous film.

The spatial control of the exchange bias both in magnitude and in direction allows to create regions characterized by different unidirectional anisotropy. In the studied exchanged bias system, at the boundary between these regions, domain walls can nucleate, whose properties can be modulated by tuning the unidirectional and uniaxial anisotropies of the film.

Novel types of domain walls, which are not energetically favored by dipolar coupling and exchange interaction, can be envisaged, paving the way to the development of new domain wall-based magnetic devices and architectures.

Acknowledgements

The authors thank Riccardo Bertacco for fruitful discussion. This work was funded by Fondazione Cariplo via project UMANA (2013-0735)

References

[1] L. F. Magaña, “Calculation of the shape of the magnetic domain wall,” *J. Magn. Magn. Mater.*, vol. 60, no. 2–3, pp. 315–318, 1986.

[2] A. Brataas, A. D. Kent, and H. Ohno, “Current-induced torques in magnetic materials,” *Nat. Mater.*, vol. 11, no. 5, pp. 372–381, 2012.

[3] D. a Allwood, G. Xiong, C. C. Faulkner, D. Atkinson, D. Petit, and R. P. Cowburn, “Magnetic domain-wall logic.,” *Science*, vol. 309, no. 5741, pp. 1688–92, Sep. 2005.

[4] S. S. P. Parkin, M. Hayashi, and L. Thomas, “Magnetic domain-wall racetrack memory.,” *Science*, vol. 320, no. 5873, pp. 190–4, Apr. 2008.

[5] M. Donolato, P. Vavassori, M. Gobbi, M. Deryabina, M. F. Hansen, V. Metlushko, B. Ilic, M. Cantoni, D. Petti, S. Brivio, and R. Bertacco, “On-chip manipulation of protein-coated magnetic beads via domain-wall conduits.,” *Adv. Mater.*, vol. 22, no. 24, pp. 2706–10, Jun. 2010.

[6] P. Bruno, “Geometrically constrained magnetic wall,” no. July, p. 4, 1999.

[7] C. C. Faulkner, “Artificial domain wall nanotraps in Ni81Fe19 wires,” *J. Appl. Phys.*, vol. 95, no. 11, p. 6717, 2004.

[8] S. Goolaup, M. Ramu, C. Murapaka, and W. S. Lew, “Transverse Domain Wall Profile for Spin Logic Applications,” *Sci. Rep.*, vol. 5, p. 9603, 2015.

[9] M. J. Benitez, M. a. Basith, R. J. Lamb, D. McGrouther, S. McFadzean, D. a. MacLaren, a. Hrabec, C. H. Marrows, and S. McVitie, “Engineering Magnetic Domain-Wall Structure in Permalloy Nanowires,” *Phys. Rev. Appl.*, vol. 3, no. 3, pp. 1–10, 2015.

[10] J. Li, “Magnetic domain structures of focused ion beam-patterned cobalt films using scanning ion microscopy with polarization analysis,” *J. Appl. Phys.*, vol. 95, no. 11, p. 6527, 2004.

[11] D. Mcgrouther, S. Mcvitie, C. H. Marrows, and J. N. Chapman, “Formation of Magnetic Structure by Domain Wall Confinement in Nanoconstriction,” vol. 47, no. 10, pp. 2511–2514, 2011.

[12] E. R. Lewis, D. Petit, L. O. Brien, J. Sampaio, A. Jausovec, H. T. Zeng, D. E. Read, and R. P. Cowburn, “Fast domain wall motion in magnetic comb structures,” vol. 9, no. October, pp. 7–10, 2010.

[13] S. Cherifi, R. Hertel, a. Locatelli, Y. Watanabe, G. Potdevin, a. Ballestrazzi, M. Balboni, and S. Heun, “Tuning the domain wall orientation in thin magnetic strips using induced anisotropy,” *Appl. Phys. Lett.*, vol. 91, no. 9, pp. 1–10, 2007.

[14] Y. P. Zhao, R. M. Gamache, G. C. Wang, T. M. Lu, G. Palasantzas, and J. T. M. De Hosson, “Effect of surface roughness on magnetic domain wall thickness, domain size, and coercivity,” *J. Appl. Phys.*, vol. 89, no. 2, pp. 1325–1330, 2001.

[15] J. Nogués and I. K. Schuller, “Exchange bias,” *J. Magn. Magn. Mater.*, vol. 192, no. 2, pp. 203–232, Feb. 1999.

[16] I. Polenciuc, a. J. Vick, D. a. Allwood, T. J. Hayward, G. Vallejo-Fernandez, K. O’Grady, and a. Hirohata, “Domain wall pinning for racetrack memory using exchange bias,” *Appl. Phys. Lett.*, vol. 162406, 2014.

[17] Y. Du, G. Pan, R. Moate, H. Ohldag, A. Kovacs, and A. Kohn, “Enhanced exchange anisotropy in IrMn/CoFeB systems and its correlation with uncompensated interfacial spins,” *Appl. Phys. Lett.*, vol. 96, no. 22, p. 222503, 2010.

[18] A. Kovács, A. Kohn, J. Dean, T. Schrefl, A. Zeltser, and M. J. Carey, “Reversal Mechanism of Exchange-Biased CoFeB / IrMn Bilayers Observed by Lorentz Electron Microscopy,” vol. 45, no. 10, pp. 3873–3876, 2009.

[19] G. Malinowski, M. Hehn, S. Robert, O. Lenoble, a. Schuhl, and P. Panissod, “Magnetic origin of enhanced top exchange biasing in Py/IrMn/Py multilayers,” *Phys. Rev. B*, vol. 68, no. 18, pp. 1–8, 2003.

[20] M. J. Donahue and D. G. Porter, *OOMMF User’s Guide, Version 1.0. Interagency Report NISTIR 6376*, vol. 3. 2004.

[21] K. O’Grady, L. E. Fernandez-Outon, and G. Vallejo-Fernandez, “A new paradigm for exchange bias in polycrystalline thin films,” *J. Magn. Magn. Mater.*, vol. 322, no. 8, pp. 883–899, Apr. 2010.

[22] J. Cho, J. Jung, K.-E. Kim, S.-I. Kim, S.-Y. Park, M.-H. Jung, and C.-Y. You, “Effects of sputtering Ar gas pressure in the exchange stiffness constant of Co40Fe40B20 thin films,” *J. Magn. Magn. Mater.*, vol. 339, pp. 36–39, Aug. 2013.

[23] B. Cui, C. Song, Y. Y. Wang, W. S. Yan, F. Zeng, and F. Pan, "Tuning of uniaxial magnetic anisotropy in amorphous CoFeB films.," *J. Phys. Condens. Matter*, vol. 25, no. 10, p. 106003, Mar. 2013.

[24] C.-Y. You, "Confined magnetic stray field from a narrow domain wall," *J. Appl. Phys.*, vol. 100, no. 4, p. 043911, 2006.

[25] a. Mougin, S. Poppe, J. Fassbender, B. Hillebrands, G. Faini, U. Ebels, M. Jung, D. Engel, a. Ehresmann, and H. Schmoranzer, "Magnetic micropatterning of FeNi/FeMn exchange bias bilayers by ion irradiation," *J. Appl. Phys.*, vol. 89, no. 11 II, pp. 6606–6608, 2001.

Figures and captions

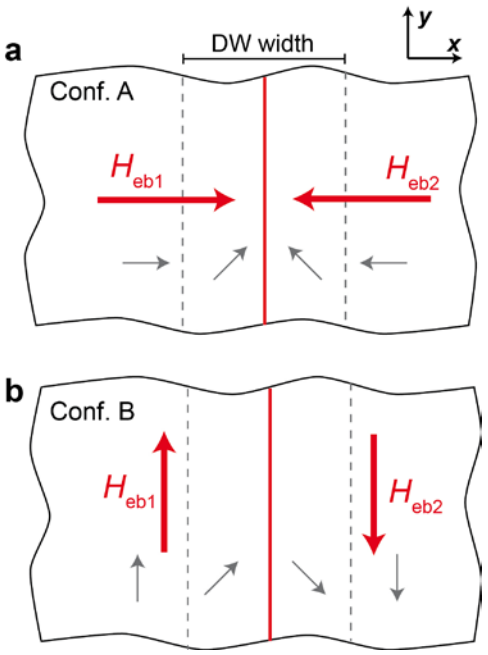

Fig. 1 Sketch of the exchange bias field (red arrows) and magnetization (grey arrows) in the two regions of the sample. The vertical solid lines mark the regions boundary; the dashed lines identify the domain wall. The exchange bias field H_{eb1} and H_{eb2} in the left and right region of the sample are oriented (a) along $+x$ and $-x$, respectively (conf. A), and (b) along $+y$ and $-y$, respectively (Conf. B).

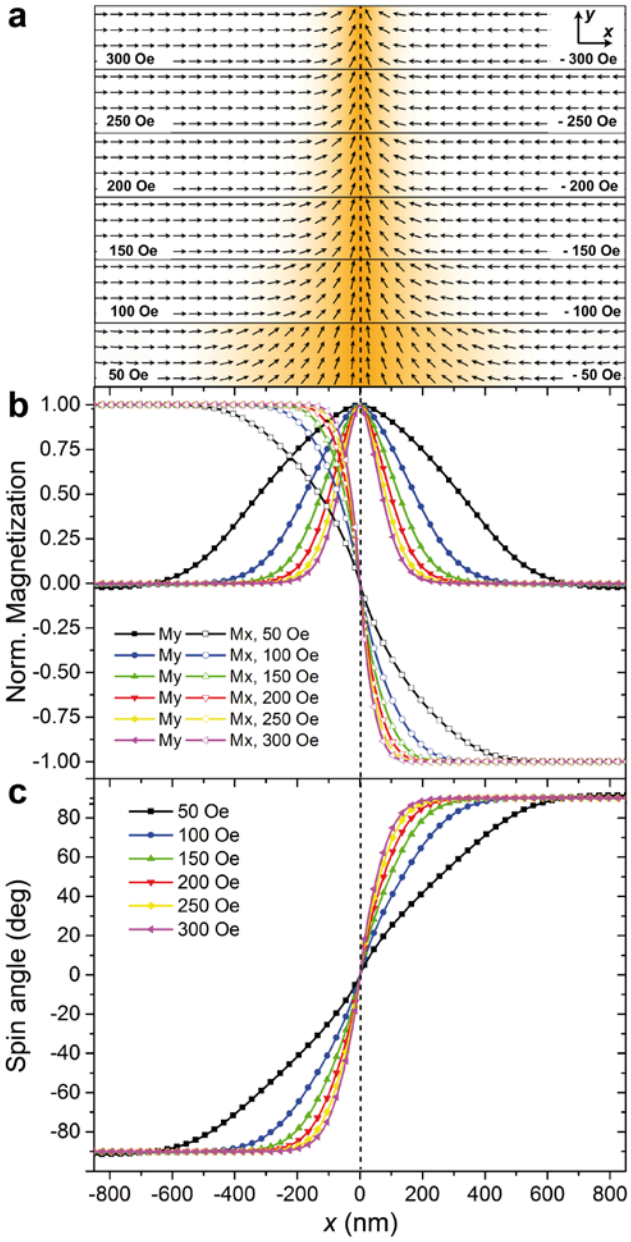

Fig. 2 a) Micromagnetic configuration of the domain wall in conf. A for different exchange bias field values along *x,* ranging from H_{eb1}= - H_{eb2} = 50 Oe to H_{eb1}= - H_{eb2} = 300 Oe. The dashed vertical line separates the two regions with opposite exchange bias. b) Normalized components of the magnetization, M_x and M_y, as a function of *x*, for different exchange bias values. c) Spin angle as a function of *x*, for different exchange bias values.

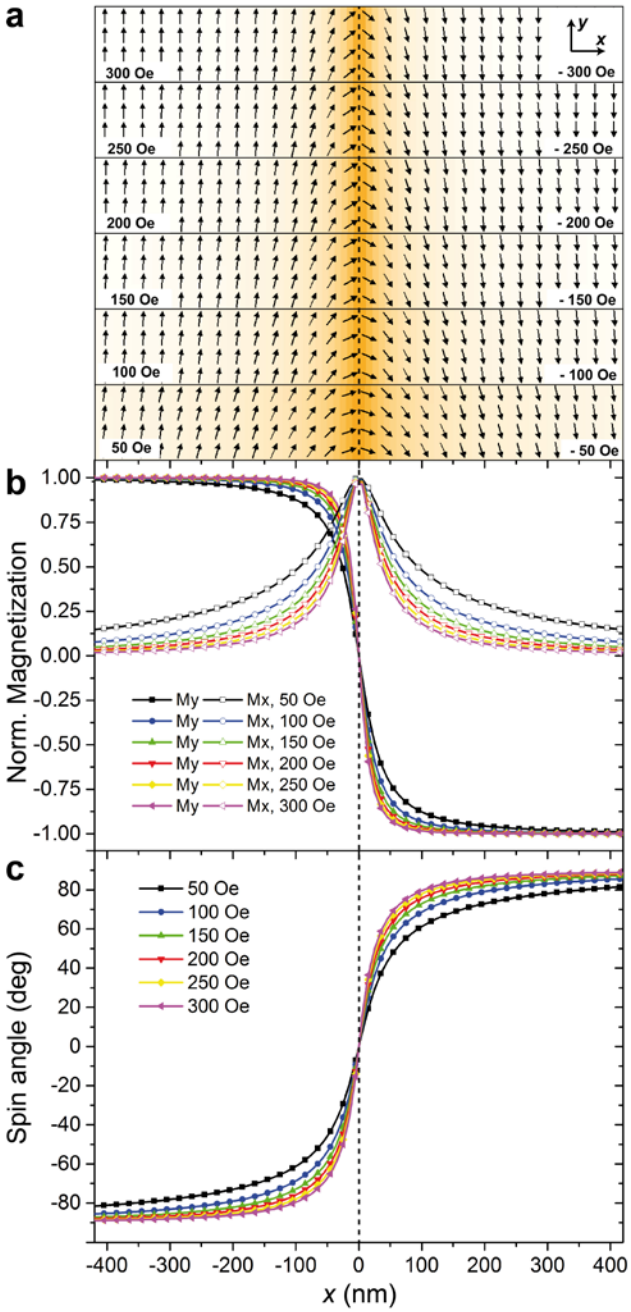

Fig. 3 a) Micromagnetic configuration of the domain wall in conf. B, for different exchange bias field values along *y,* ranging from H_{eb1}= - H_{eb2} = 50 Oe to H_{eb1}= - H_{eb2} = 300 Oe. The dashed vertical line separates the two regions with opposite exchange bias. b) Normalized components of M_x and M_y, as a function of *x*, for different exchange bias values. c) Spin angle as a function of *x*, for different exchange bias values.

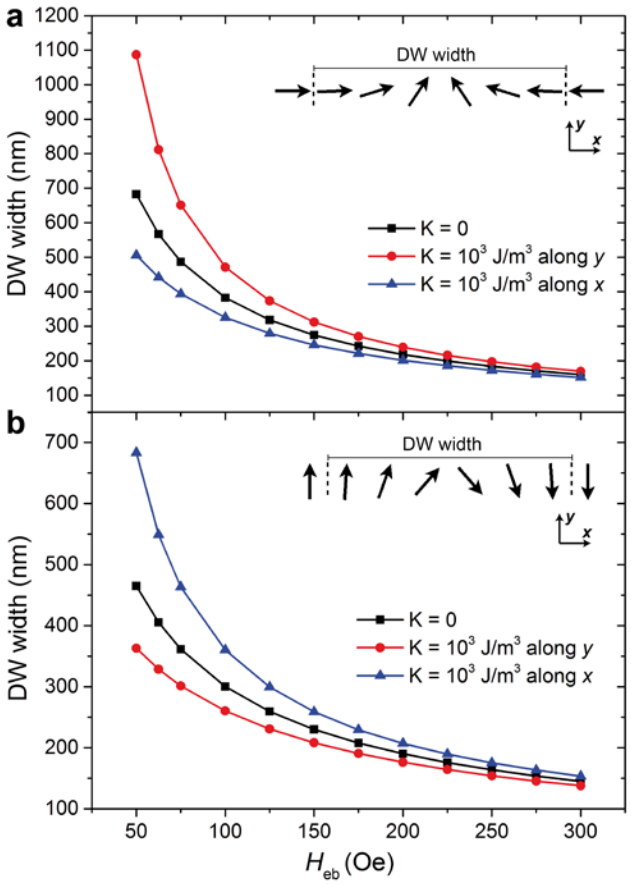

Fig. 4 Domain wall width as a function of the exchange bias field, in conf. A a) and in conf. B b), respectively. Different values of the anisotropy constant *K* and orientation for the easy anisotropy axis were considered.

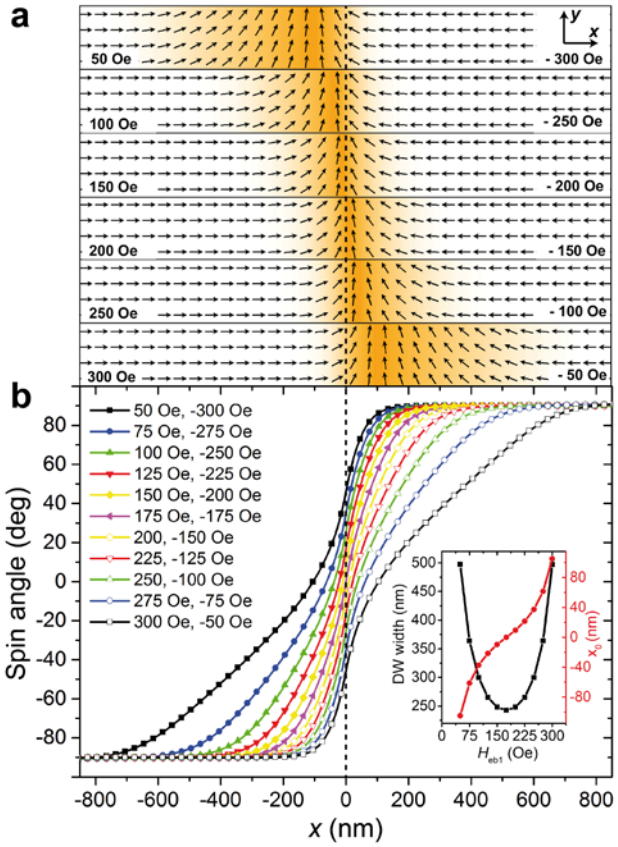

Fig. 5 a) Micromagnetic configuration of the domain wall in conf. A for different exchange bias field values along *x,* ranging from H_{eb1}=50 Oe, H_{eb2}=-300 Oe to H_{eb1}=300 Oe, H_{eb2}=-50 Oe. The dashed vertical line separates the two regions with exchange bias oriented in the opposite directions. b) Spin angle as a function of *x*, for different exchange bias values. In the inset, domain wall width and position x_0 of the domain wall center (where $M_x = 0$) as a function of H_{eb1}.

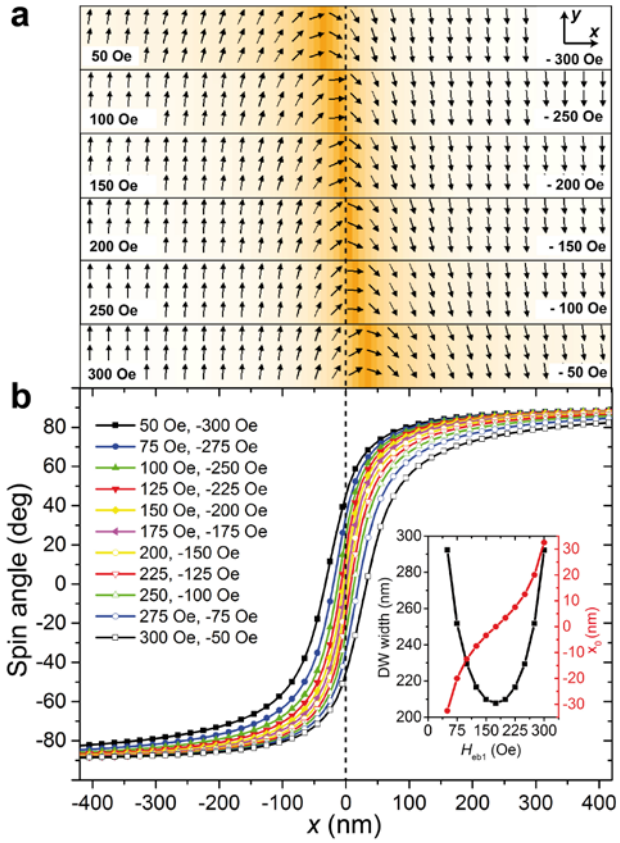

Fig. 6 a) Micromagnetic configuration of the domain wall in conf. B for different exchange bias field values along *y,* ranging from H_{eb1}=50 Oe, H_{eb2}=-300 Oe to H_{eb1}=300 Oe, H_{eb2}=-50 Oe. The dashed vertical line separates the two regions with exchange bias oriented in the opposite directions. b) Spin angle as a function of *x*, for different exchange bias values. In the inset, domain wall width and position x_0 of the domain wall center (where $M_y = 0$) as a function of H_{eb1}.